International Journal of Heat and Mass Transfer 68 (2014) 444–455

Contents lists available at ScienceDirect

International Journal of Heat and Mass Transfer

journal homepage: www.elsevier.com/locate/ijhmt

Convection in a horizontal fluid layer under an inclined temperature gradient for Prandtl numbers $Pr > 1$

A.S. Ortiz-Pérez, L.A. Dávalos-Orozco *

Instituto de Investigaciones en Materiales, Departamento de Polímeros, Universidad Nacional Autónoma de México, Ciudad Universitaria, Circuito Exterior S/N, Delegación Coyoacán, 04510 México D. F., México

ARTICLE INFO

Article history:
Received 19 February 2013
Received in revised form 24 September 2013
Accepted 24 September 2013
Available online 18 October 2013

Keywords:
Thermal convection
Inclined temperature gradient
Pattern formation
Hadley circulation
Atmospheric flows

ABSTRACT

In this paper calculations are done of the flow instability of a shallow horizontal fluid layer under an inclined temperature gradient for Prandtl numbers of magnitudes $Pr > 1$. In a previous paper (Ortiz-Pérez and Dávalos-Orozco, 2011 [17]), the range of values investigated were $Pr \leqslant 1$. There, the magnitudes of the horizontal Rayleigh number investigated were far larger than those used in the literature and it was found the new oblique oscillatory mode *Obo*. In the present paper it is found that this oblique oscillatory mode still appears for $Pr = 2$. Further, it is also shown that some modes become irrelevant when the Prandtl number is increased, and different modes become the first to go unstable. An important result is that above a large enough Prandtl number, the curves of criticality remain almost the same. Therefore, the limit $Pr \to \infty$ is employed to calculate useful analytical expressions for the longitudinal modes of criticality which cover almost all the range of horizontal Rayleigh numbers. In contrast to the authors previous results, in this paper it is shown that for $Pr > 1$ the transversal oscillatory mode has a range, in the horizontal Rayleigh number, as the first unstable one which first increases and then decreases with Pr, but never disappears.

1. Introduction

Temperature differences are unavoidable in many natural phenomena. They are responsible of a variety of convection motions. In industrial applications it is sometimes necessary to avoid any motion as in processes of crystal growth [1] and solidification of molten metals [2]. The most simple convective motion is that of a horizontal fluid layer heated from below. This has been reviewed in the monograph by Chandrasekhar [3]. In this particular problem the fluid starts in a hydrostatic state. In contrast, if the fluid is heated at one of the lateral boundaries, a closed main flow appears forming one large cell. The creation of that cell is due to the upward motion of the fluid by buoyancy force at the hot wall and its downwards motion at the cold wall, satisfying mass conservation. The motion is sustained by a horizontal temperature gradient which destabilizes the flow when its magnitude is above a critical one. This closed flow is called Hadley circulation [4]. For small aspect ratios (very far away lateral walls), the stability of the Hadley circulation was investigated by Hurle et al. [1] and Hart [4]. Kuo et al. [5] present important corrections to previous works by including a very large range of Prandtl numbers. In other papers Kuo et al. [6] and Wang et al. [7] investigated the nonlinear problem for particular ranges of the Prandtl number, taking into account very good conducting and insulating walls. Numerical calculations and corrections to previous results were also done by Laure [8] and Laure and Roux [9]. Hughes and Griffiths [10] reviewed this problem including applications to oceanography.

In nature temperature gradients do not appear as purely horizontal or purely vertical, but a combination of both. Therefore, it is worth considering the effect of an inclined temperature gradient. Weber [11] investigated the problem assuming that the horizontal walls are stress-free and that the horizontal temperature gradient is small. Later Sweet et al. [12] investigated the instability for free shear walls and found the possibility of oscillatory convection increasing the ratio of the applied temperature gradients. This problem was extended for small horizontal temperature gradient and rigid horizontal walls by Bhattacharyya and Nadoor [13]. Weber [14] improved his previous calculations for stress-free walls using a Galerkin method. He also made calculations for rigid horizontal walls and found that the Prandtl number is important to determine which mode is the first to appear in the instability, the longitudinal or the transversal one with respect to the main flow. Besides, he showed that an increase of the horizontal temperature gradient promotes oscillatory instabilities. Nield [15] was the first to give a more complete view of this phenomena for four different values of the Prandtl number. His goal was to investigate all the possible modes of instability by means of a Galerkin method.

* Corresponding author. Tel.: +52 5556224601; fax: +52 5556161201.
E-mail address: ldavalos@unam.mx (L.A. Dávalos-Orozco).

0017-9310/$ - see front matter © 2013 Elsevier Ltd. All rights reserved.
http://dx.doi.org/10.1016/j.ijheatmasstransfer.2013.09.065

Nomenclature

a_n	nth constant Galerkin coefficient
b_n	nth constant Galerkin coefficient
c_n	nth constant Galerkin coefficient
d	thickness of the layer
d_n	nth constant Galerkin coefficient
D/DT	Lagrange operator
$D = d/dz$	symbol of z-derivative
f_n	nth constant Galerkin coefficient
g	acceleration of gravity
g_n	nth constant Galerkin coefficient
k	x-direction wavenumber
k	vertical unit vector
l	y-direction wavenumber
Lo1	longitudinal oscillatory mode
Ls1	first longitudinal stationary mode
Ls2	second longitudinal stationary mode
Obo	oblique mode
p′	pressure perturbation
Pr	Prandtl number
R_V	vertical Rayleigh number
R_{VC}	vertical critical Rayleigh number
R_H	horizontal Rayleigh number
$T(x,z)$	main temperature profile
	T': nondimensional temperature
To	transversal oscillatory mode
Ts	transversal stationary mode
$\bar{u}' = (u', v', w')$	nondimensional velocity perturbation
$u(z)$	x-direction perturbation amplitude
$U(z)$	x-direction main flow
u_e	x-direction even Galerkin velocity
u_o	x-direction odd Galerkin velocity
$V(z)$	y-direction main flow
$w(z)$	z-direction perturbation amplitude
w_e	z-direction even Galerkin velocity
w_o	z-direction odd Galerkin velocity

Greek

α	wavenumber magnitude
α_C	critical wavenumber magnitude
α_T	coefficient of volumetric expansion
β_H	horizontal temperature gradient
ΔT	vertical temperature difference
θ	amplitude of temperature perturbation
θ_e	even Galerkin temperature
θ_o	odd Galerkin temperature
κ	thermal diffusivity
ν	kinematic viscosity
ρ_0	reference density
σ	frequency of oscillation
σ_C	critical frequency of oscillation
ϕ	perturbation propagation angle
ϕ_C	perturbation critical propagation angle

Numerical problems limited his results to a horizontal Rayleigh number of 6000. Later, Kaloni and Qiao [16] made calculations of the nonlinear problem by means of the energy method. They showed that the curves of criticality of Nield [15], which did not drop to a zero critical vertical Rayleigh number R_{VC}, should do so with an increase of the horizontal Rayleigh number R_H. Therefore, for some Prandtl numbers the linear results of Nield [15] have to be corrected and extended to larger magnitudes of R_H.

In this paper we present new results of the linear problem of natural convection under an inclined temperature gradient when the Prandtl number is larger than one. Here, it is also of interest to find out the magnitude of Pr around which the oblique mode may disappear (see [17]). Furthermore, it is shown that the transverse oscillatory mode, found by Nield [15], decreases its range in R_H as the most unstable one by increasing *Pr*. However, it never disappears. The improved numerical method used by Ortiz-Pérez and Dávalos-Orozco [17] cleared the restriction on the magnitude of the Prandtl number, which now may be as large as needed. Here, the calculated curves of criticality drop until the critical vertical Rayleigh number R_{VC} is zero, in good agreement with previous results in the literature with horizontal temperature gradient alone.

The paper is organized as follows. In Section 2 a description of the physical system is given along with the equations of motion and energy with their linear version for use in the numerical analysis. In Section 3 a description of the numerical method is presented with a discussion of how it improves the one used by Nield [15]. Section 4 gives the results in the form of plots of the critical vertical Rayleigh number R_{VC}, wavenumber a_C, frequency of oscillation σ_C and angle of propagation of the perturbation ϕ_C against R_H, the horizontal Rayleigh number. Also Section 4 gives the results of an asymptotic expansion analysis in terms of a large Prandtl number. Section 5 presents the discussion and conclusions. The Appendix A contains the calculation details of the very useful and simple approximate formulas for the marginal R_V of the two longitudinal modes. These modes are shown to be dominant in almost all the range of R_H investigated when the Prandtl number is larger enough. The Appendix B shows the validity and convergence of the numerical algorithm used in this and in the authors previous paper.

2. Equations of motion

In this paper it is supposed that a fluid layer is contained between two parallel very good conducting solid walls perpendicular to gravity (anti parallel to the z-direction, see Fig. 1) that have an imposed horizontal temperature gradient superposed to a vertical one due to heating from the lower wall. The horizontal temperature gradient is due to the existence of a hot and a cold lateral vertical walls located very far away from the middle region of interest here. The buoyancy force makes the fluid to move upwards in the hot wall and downwards in the cold wall. Due to mass conserva-

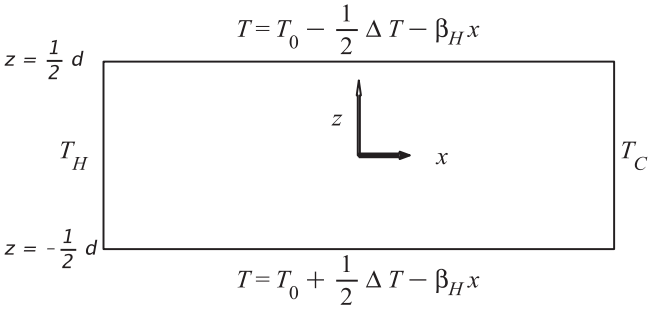

Fig. 1. Sketch of the system. The liquid layer is contained between two horizontal walls separated a distance d. There are vertical and horizontal temperature gradients. The temperature difference between lower and upper solid walls is ΔT. β is the rate of uniform temperature increase along the x-axis. The lateral walls are located at a very larger distance from the region under study.

tion, the main flow is generated in the form of one very large convection cell. If the distance between the lateral walls is very large in comparison with the thickness of the layer, the main velocity profile in the middle region between them can be considered as parallel flow in the x-direction with the form $U(z)$. Note that the instability is three dimensional and that perturbations perpendicular to the main flow (in the x-direction) are also investigated. The equations of motion, heat diffusion and mass conservation are, respectively:

$$Pr^{-1}\frac{D\bar{u}'}{Dt} = -\nabla p' + T'\mathbf{k} + \nabla^2\bar{u}' \tag{1}$$

$$\frac{DT'}{Dt} = \nabla^2 T' \tag{2}$$

$$\nabla\cdot\bar{u}' = 0 \tag{3}$$

where use is made of the Boussinesq approximation. Here, $\bar{u}' = (u',v',w')$ is the velocity vector, $\mathbf{k}$ is a vertical unit vector, p' is the pressure, T' is the temperature and D/Dt is the Lagrange operator. The variables have been made non dimensional using for distances the thickness of the layer d, for time d^2/κ (where κ is the thermal diffusivity), for velocity κ/d, for pressure $\rho_0\kappa\nu/d^2$ (where ρ_0 is a reference density) and for temperature $\Delta T/R_V$, where ΔT is the vertical temperature difference and the vertical Rayleigh number is defined as $R_V = g\alpha_T d^3\Delta T/\nu\kappa$. The horizontal Rayleigh number is defined as $R_H = R_V d\beta_H/\Delta T = g\alpha_T d^4\beta_H/\nu\kappa$, where g is the acceleration of gravity, α_T is the coefficient of volumetric expansion and β_H is the rate of uniform temperature increase along the x-axis. The walls are assumed to be rigid and very good conductors. Then the velocity and temperature satisfy the boundary conditions at the walls located at $z = \pm 1/2$

$$\bar{u}' = 0 \tag{4}$$

$$T' = \mp R_V/2 - R_H x \tag{5}$$

As explained above, the interest here is on the instability of the parallel flow in the middle region of the layer, very far from the lateral walls. This flow has a steady solution which depends only on the variable z. At the same time, the temperature depends on the velocity profile. Then, the steady parallel flow equations are:

$$D^3U(z) = -R_H \tag{6}$$

$$D^3V(z) = 0 \tag{7}$$

$$D^2T(x,z) = -R_H U(z) \tag{8}$$

Here, use is made of the operator $D = d/dz$. An extra condition seems to be missing because the differential equations (6) and (7) are of third order. The condition used in this case is that the integrals of $U(z)$ and $V(z)$ in the range $-1/2 \leqslant z \leqslant 1/2$ must be zero (that is, the mass flux per unit length is zero). Thus, the main flow and temperature solutions are:

$$U(z) = R_H\left(\frac{z}{24} - \frac{z^3}{6}\right) \tag{9}$$

$$V(z) = 0 \tag{10}$$

$$T(x,z) = R_H^2\left(\frac{7z}{5760} - \frac{z^3}{144} + \frac{z^5}{120}\right) - R_V z - R_H x \tag{11}$$

Analytic temperature profiles, like that of Eq. (11), have been reviewed by Lappa [18], under different physical conditions. The perturbation of the variables is assumed in the form of normal modes $G(z)exp[i(kx + ly - \sigma t)]$, where $G(z)$ represents the amplitude of any of the perturbations and k and l are the x and y-components of the wavenumber. σ is a complex number whose real part is the frequency of oscillation of the perturbation and its imaginary part is the growth rate. Substitution into the perturbed equations gives [15,17]:

$$[Pr(D^2-\alpha^2) - i(kU-\sigma)](D^2-\alpha^2)w + ikwD^2U - Pr\alpha^2\theta = 0 \tag{12}$$

$$[(D^2-\alpha^2) - i(kU-\sigma)]\theta + R_H u - wDT = 0 \tag{13}$$

$$[Pr(D^2-\alpha^2) - i(kU-\sigma)](-\alpha^2 u + ikDw) + l^2 wDU = 0 \tag{14}$$

where u and w are the amplitudes of the x and z-components of the velocity perturbations, respectively, and θ is the amplitude of the temperature perturbation. $\alpha^2 = k^2 + l^2$ is the square of the magnitude of the wavenumber vector, which is useful when it is expressed in polar form by means of $k = \alpha\cos\phi$ and $l = \alpha\sin\phi$, where ϕ is the angle of propagation of the perturbation with respect to the direction of the main flow. When the walls are rigid and the temperature is fixed, the boundary conditions are $w = Dw = u = \theta = 0$ at $z = \pm 1/2$.

3. Numerical analysis

The system of equations Eqs. (12) and (13), is the same as in Ortiz-Pérez and Dávalos-Orozco [17]. Again, a numerical Galerkin method [19,20] is used, in which even and odd modes are included at the same time in the process (see Hart [21]). This allowed us to improve the results of Nield [15] and increase the magnitude of the horizontal Rayleigh number to find the oscillatory oblique mode as the first unstable one in a range of R_H [17]. It will be shown presently that this mode only survives in a limited range of Pr.

The expansions of the variables which are substituted into the homogeneous system of differential Eqs. (12)–(14) are used in the numerical analysis are:

$$w = w_e + w_o = \sum_{n=1}^{N}[a_{2(n-1)}z^{2(n-1)}(z^2-1/4)^2 + b_{2n-1}z^{2n-1}(z^2-1/4)^2] \tag{15}$$

$$\theta = \theta_e + \theta_o = \sum_{n=1}^{N}[c_{2n-1}cos(2n-1)\pi z + d_{2n}sin2n\pi z] \tag{16}$$

$$u = u_e + u_o = \sum_{n=1}^{N}[f_{2n-1}cos(2n-1)\pi z + g_{2n}sin2n\pi z] \tag{17}$$

where the subindexes e and o mean even and odd functions, respectively (see reference [17] for more details).

In the previous paper [17] it was shown that the system of Eqs. (12)–(14), has some symmetries which can be used to understand the instability in the 360° range of the angle ϕ by only doing calculations in the first quadrant, that is, from 0° to 90°. Therefore, the calculations of the oblique mode presented in this paper are also limited to this range.

As done before, the results of the numerical analysis were compared with those reported for the case of $R_V = 0$ (see Kuo et al. [5]). Even more, the convergence of the numerical algorithm was checked increasing the order of the Galerkin method in a wide range of magnitudes of the Prandtl number (see Appendix B).

4. Numerical results

The numerical results are presented in the form of plots of the critical values against the horizontal Rayleigh number. Only when the oblique mode is the first unstable one, a fourth figure is given for the critical angle of propagation of the perturbation. Other results where only longitudinal and transversal modes are present do not need that figure. Therefore, the following notation will be used in the paper. The longitudinal mode means a roll aligned with the flow direction, here the x-direction. In the present problem, there are three longitudinal modes, the oscillatory $Lo1$, the first stationary $Ls1$ and second stationary $Ls2$ modes. The transversal mode

means a roll in a direction perpendicular to the flow direction, that is the y-direction. There are two transversal modes, the stationary *Ts* and the oscillatory *To* modes. There is also the new oblique oscillatory mode *Obo* which is a roll making an angle with respect to the x-direction. This angle depends on the magnitude of the horizontal Rayleigh number, as will be shown presently.

The marginal curves were calculated fixing Pr, R_H and the wavenumber. When the mode is stationary, the roots R_V were calculated from the determinant found with the Galerkin method. There are a number of roots and only the smallest one is selected. The process follows by varying the wavenumber until a minimum is found for R_V. For fixed Pr and R_H, this is called the critical R_{VC} corresponding to the critical wavenumber α_C. If the flow is oscillatory, the determinant is complex. Therefore, before calculating the roots R_V of the real part, the marginal frequency of oscillation is obtained as the root of the imaginary part. This is substituted into the real part from which the roots R_V are obtained. From them, only the smallest one is the marginal. The process follows by varying the wavenumber until the minimum for R_V is obtained. For fixed Pr and R_H, this is called the critical R_{VC} corresponding to the critical wavenumber α_C and frequency σ_C. In particular, the oblique oscillatory mode was calculated by searching, around any stationary or oscillatory curve of criticality, where a more unstable mode may appear at different angles of the perturbation wavenumber. With this method were found all the important modes of instability.

Fig. 2(a) shows the critical values of R_{VC} against R_H for $Pr = 2$. Saturated liquid amonia [22] has a Pr around 2 at -30 °C. Modes that were not the first unstable ones for low Pr, now are the first to appear for almost the whole range of R_H. In Fig. 2 the instability is dominated by the longitudinal stationary modes *Ls*1 and *Ls*2 and the oscillatory mode *Lo*1. As seen in the middle of the R_H axis, the range of the oblique oscillatory mode *Obo* has been reduced. Also notice that in a range of R_H, the transverse oscillatory mode *To* is already close to the lowest curves of criticality. Therefore, it is possible that it becomes the first unstable one with a small increase of Pr. The *Ls*1 mode starts to be the first unstable one with $R_{VC} = 1708$ at $R_H = 0$. Then, from $R_H = 2884$, the oscillatory longitudinal mode *Lo*1 becomes the first one. A codimension two point appears between them with the critical values given in the following order (R_H,R_V,α,σ): (2884, 11519.92, 5.4, 0) and (2884, 11519.92, 2.7,

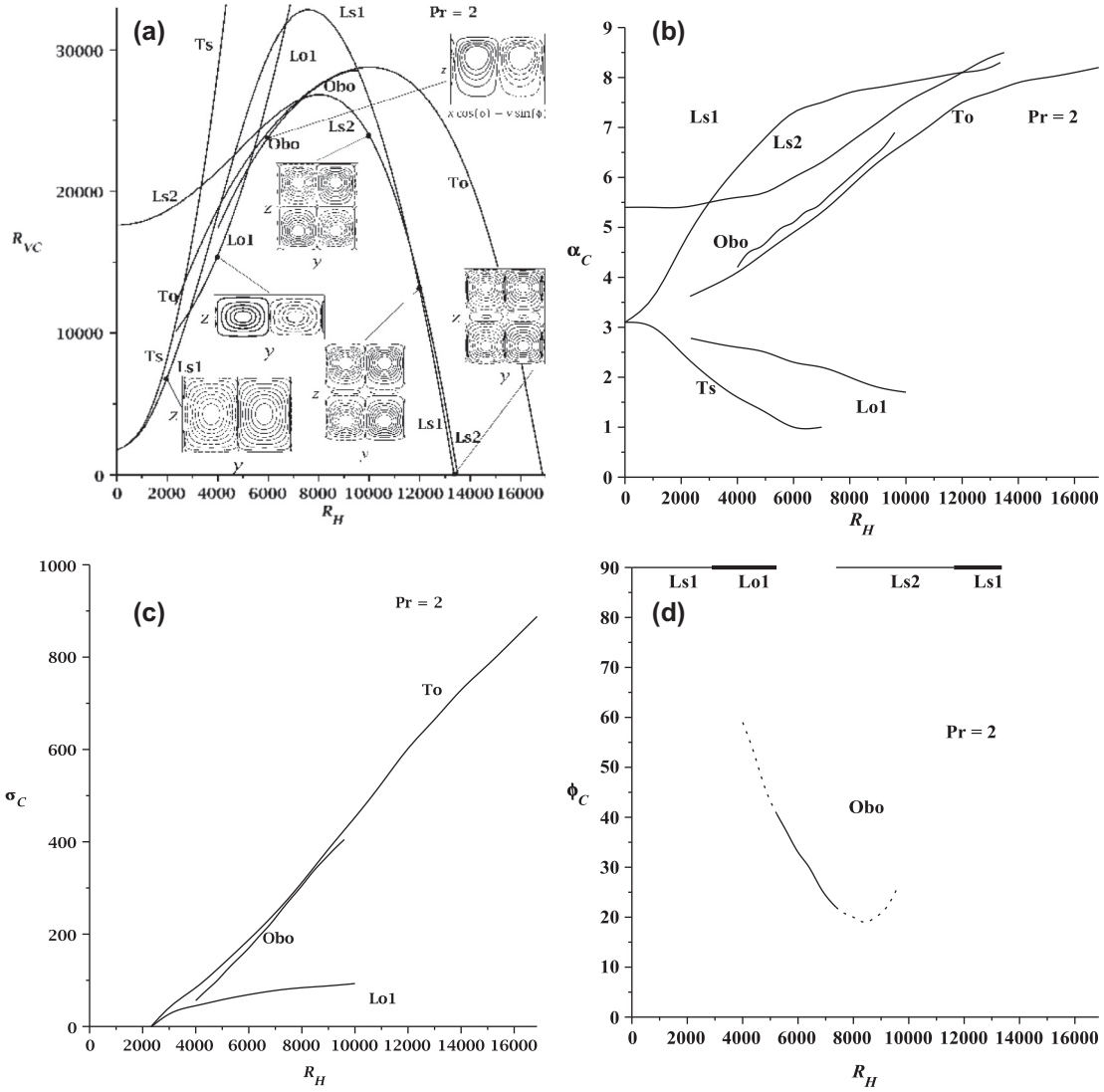

Fig. 2. Graphs of R_{VC},α_C,σ_C and ϕ_C vs R_H for Pr = 2. In (a), the first unstable mode is *Ls*1, then from $R_H = 2884$, the mode *Lo*1, next from $R_H = 5225$, the mode *Obo*, from $R_H = 7374$ follows the mode *Ls*2 and finally from $R_H = 11632.5$, the mode *Ls*1. Two codimension two points appear: one between *Ls*1 and *Lo*1 when $R_H = 2884$, another one between *Obo* and *Ls*2 when $R_H = 7374$. The mode *Ls*1 is the first to decrease and touch the horizontal axis ($R_{VC} = 0$) when $R_H = 13360.36$. Figures (b)–(d) show critical wavenumber, frequency and angle of propagation against R_H. The streamlines correspond to values in the order (R_H,R_{VC},α_C,σ_C): *Ls*1 (2000, 6866, 4.6, 0), *Lo*1 (4000, 15496.85, 2.6, 45.27), *Obo* (6000, 23826.13, 5.1, 170.74) at 33°, *Ls*2 (10000, 23935.48, 7.5, 0.0), *Ls*1 (12000, 13070.79, 8.1, 0) and *Ls*1 (13360.36, 0, 8.3, 0).

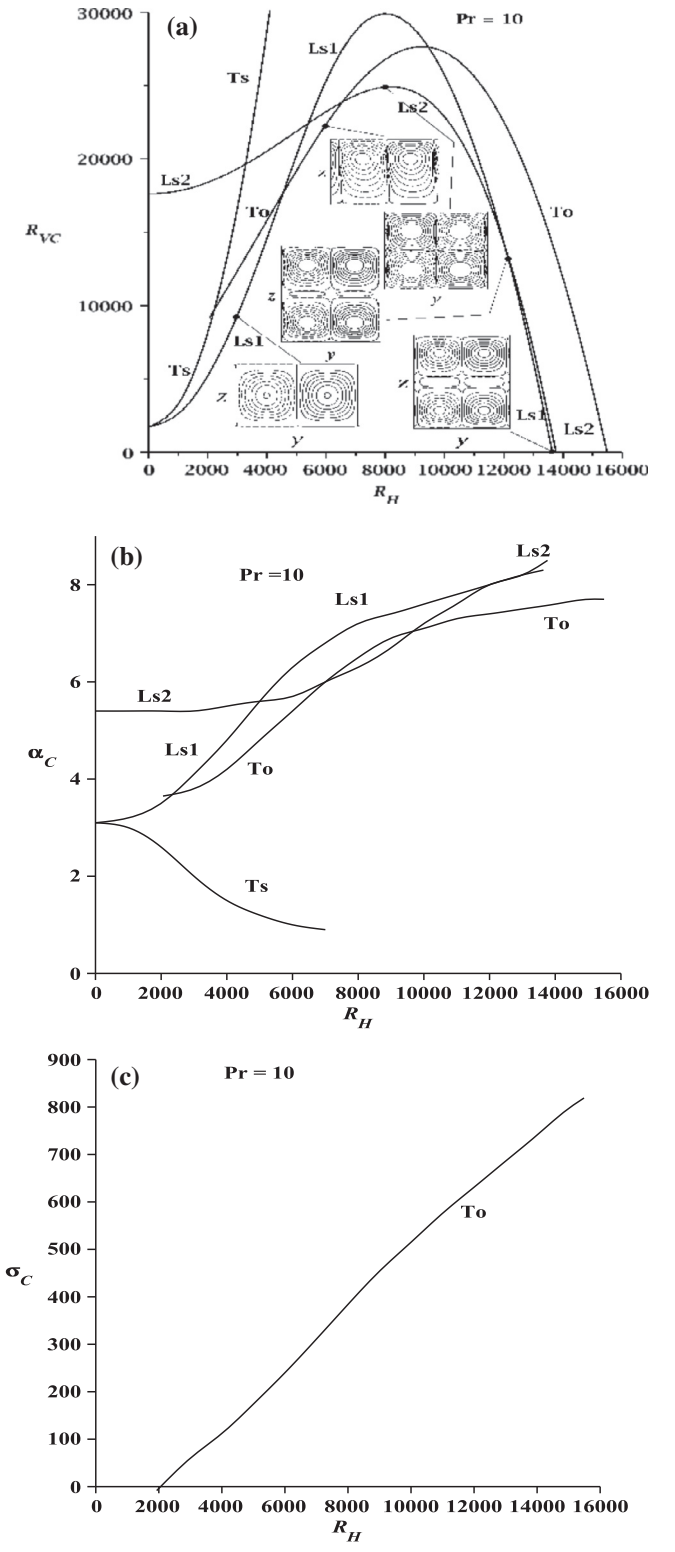

Fig. 3. Graphs of R_{VC},α_C, and σ_C vs R_H for Pr = 10. In Fig. (a), *Ls*1 is the first unstable mode. From R_H = 4538.5 is the mode *To*. From R_H = 6548 is the mode *Ls*2. Finally, from R_H= 12039.8 is the mode *Ls*1. *Ls*1 drops to R_{VC} = 0 at R_H = 13641.77. Figs. (b) and (c) present the critical wavenumber and frequency, respectively. The streamlines data, in the order (R_H,R_{VC},α_C,σ_C), are: *Ls*1 (3000, 9311.87, 4.1, 0), *To* (6000, 22366.89, 5.4, 240.31), *Ls*2 (8000, 24388.35, 6.2, 0), *Ls*1 (12100, 13445. 38, 8, 0) and *Ls*1 (13641.77,0, 8.3, 0).

24.82) for *Ls*1 and *Lo*1, respectively. The mode *Lo*1 plays a important role in the instability for Pr = 2. For higher Prandtl numbers *Lo*1 is more stable than the others. This is clear by observing the continuous increase of its slope as the Prandtl number is increased [17]. The oblique mode *Obo* is the first unstable one from (5525, 21700.59, 4.8, 124.11) at 41° and *Lo*1 has the values (5525, 21700.59, 2.5, 61.91). Another codimension two point appears when the *Obo* and *Ls*2 cross to each other at the points (7374, 26591.92, 5.7, 261.49) and 23°, and (7374, 26591.92, 6.4, 0), respectively. The mode *Ls*1 is intersected by *Ls*2 at (11632.5, 16053.48, 8.1, 0) and (11632.5, 16053.48, 8, 0), respectively. Finally, the *Ls*1 decreases until R_{VC} = 0 at R_H = 13360.36 with α = 8.3. Notice that a little far (more stable) from *Ls*1 is *Ls*2 touching the axis at R_H = 13499, with wave number α = 8.5.

Fig. 3(a) presents the critical values R_{VC} against R_H for Pr = 10, corresponding approximately to saturated liquid water [22] at 10°C. Notice the importance of the longitudinal stationary modes *Ls*1 and *Ls*2 for almost all range of R_H. In that figure there is also a range where the oscillatory transverse mode *To*, first found by Nield [15], is important. *To* is the first unstable one in the range $4538.5 \leqslant R_H \leqslant 6548$. *Ls*1 is the first unstable one from R_H = 0 to R_H = 4538.5. The first codimension two point occurs between modes *Ls*1 and *To* when R_H = 4538.5 at (4538.5, 17641. 42, 5.22, 0) for *Ls*1 and at (4538.5, 17641.42, 4.51, 144.76) for *To*. There are differences in the magnitudes of the wavenumbers. From R_H = 6548 the mode *Ls*2 is the first unstable one until R_H = 12039.8, where *Ls*1 becomes the first one. Thus, a second codimension two point occurs at R_H = 6548 between modes *To* and *Ls*2 at (6548, 23890.02, 5.75, 279.79) for *To* and (6548, 23890.02, 5.84, 0) for *Ls*2. The intersection between *Ls*2 and *Ls*1 occurs at (12039.8, 14026.42, 7.95, 0) for *Ls*2 and (12039.8, 14026.42, 7.98, 0) for *Ls*1, which can be considered the same. In this way, mode *Ls*1 plays an important role in two large ranges of R_H. *Ls*1 drops to R_{VC} = 0 at (13641.77, 0, 8.3, 0). Behind mode *Ls*1, the curves of *Ls*2 and *To* drop for larger magnitudes of R_H. The curves of the other critical values are presented in Fig. 3(b) for the critical wavenumber and in Fig. 3(c) for the critical frequency.

Now, the Prandtl number is increased as in Fig. 4(a) which presents the case for Pr = 100, corresponding approximately to a hydraulic fluid (MIL-H-5606) [22] at 75°C. Notice that *Ls*1 increases its range of R_H as the most unstable one. However, that increase is relatively small, almost 30 units. The oscillatory transverse mode *To* has reduced its influence as a critical curve and now it is limited to appear in the small range from R_H = 5434 to R_H = 5849. Therefore, the two codimension two points are closer than in Fig. 3 for Pr = 10. The first codimension two point appears at *Ls*1 (5434, 21212.30, 5.32, 0) and *To* (5434, 21212.30, 5.18, 214.36) and the second one at *To* (5849, 22651.01, 5.47, 244.1) and *Ls*2 (5849, 22651.01, 5.64,0). The modes *Ls*1 and *Ls*2 cross to each other at *Ls*1 (12113.9, 13677.10, 7.95,0) and *Ls*2 (12113.9, 13677.10, 7.91, 0) which practically are the same magnitudes. From R_H = 0 to R_H = 5434 the first unstable mode is *Ls*1. From the second codimension two point the mode *Ls*2 is the first unstable one up to the intersection with *Ls*1. *Ls*1 drops to R_{VC} = 0 at R_{HC} = 13704 with a wave number α_C = 8.3. The Fig. 4(a) also presents plots of the streamlines at different representative locations. The critical wavenumbers and frequencies are shown in Fig. 4(b) and (c), respectively.

It is of interest to know what happens at very large Prandtl numbers. Therefore, Fig. 5(a) presents results for Pr = 500, which corresponds to a hydraulic fluid (MIL-H-5606) [22] at 0°C. The plots are very similar to Pr = 100. However, an important difference appears. The oscillatory transverse mode *To* now has a very narrow range to be the first unstable one. That is, between R_H = 5564 to R_H = 5793. Notice that both stationary longitudinal modes, *Ls*1 and *Ls*2, have covered almost the whole range of R_H. At the same time, both codimension two points have moved more closer to each other. The first codimension two point appears at

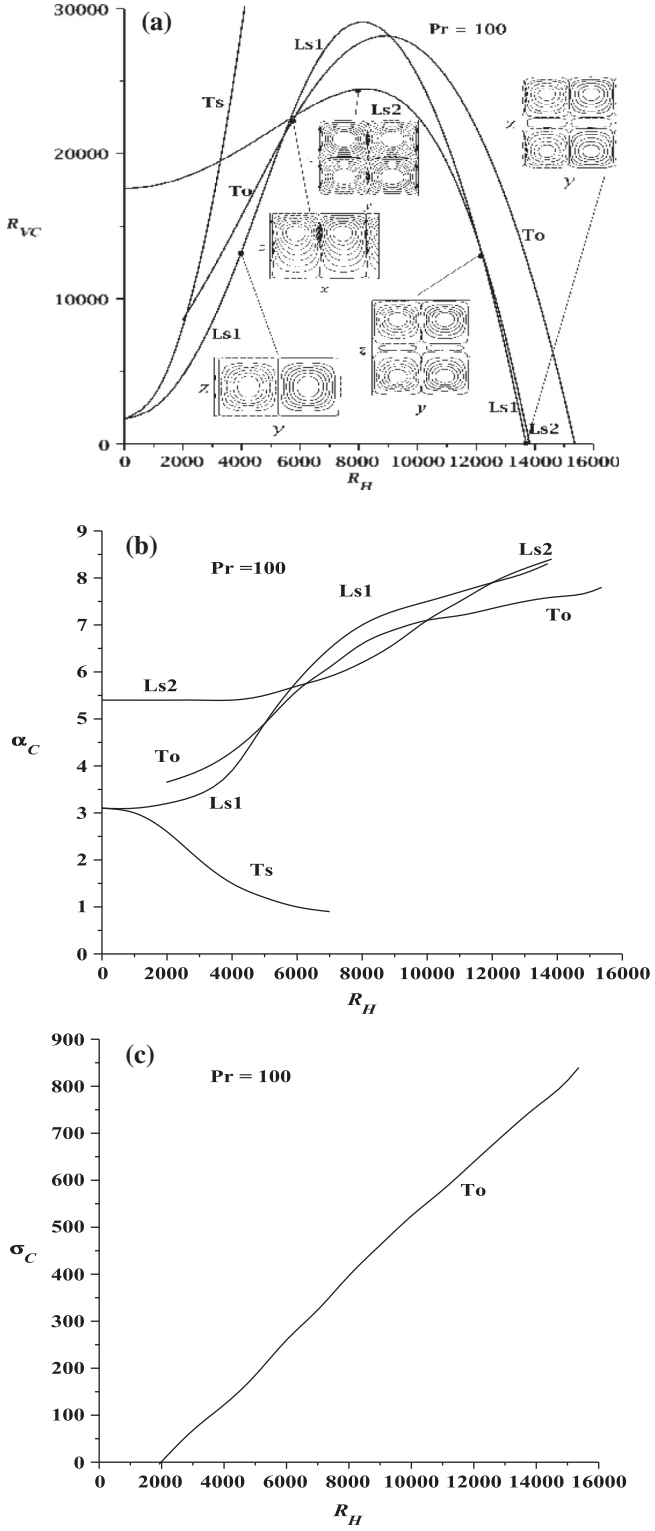

Fig. 4. Graphs of R_{VC}, α_C, and σ_C vs R_H for Pr = 100. In Fig. (a) *Ls*1 is the first unstable mode, next from R_H = 5434, it is the oscillatory transverse mode *To*. From R_H = 5849 it follows *Ls*2 and from R_H = 12113.9 it is again *Ls*1. The first codimension two point between *Ls*1 and *To* appears at R_H = 5434. A second codimension two point between *To* and *Ls*2 occurs at R_H= 5849. The intersection between *Ls*2 and *Ls*1 occurs at R_H = 12113.9, after which *Ls*1 is again the first unstable one. *Ls*1 falls to R_{VC} = 0 at R_H = 13704.27. Figs. (b) and (c) present the critical wavenumbers and frequencies. The plots of the streamlines correspond to the values: *Ls*1 (4000, 13269.41, 3.9,0), *To* (5700, 22230.38, 5.4, 235.31), *Ls*2 (8000, 24388.35, 6.2, 0), *Ls*1 (12150, 13825.63, 8, 0) and *Ls*1 (13704.27, 0, 8.3, 0).

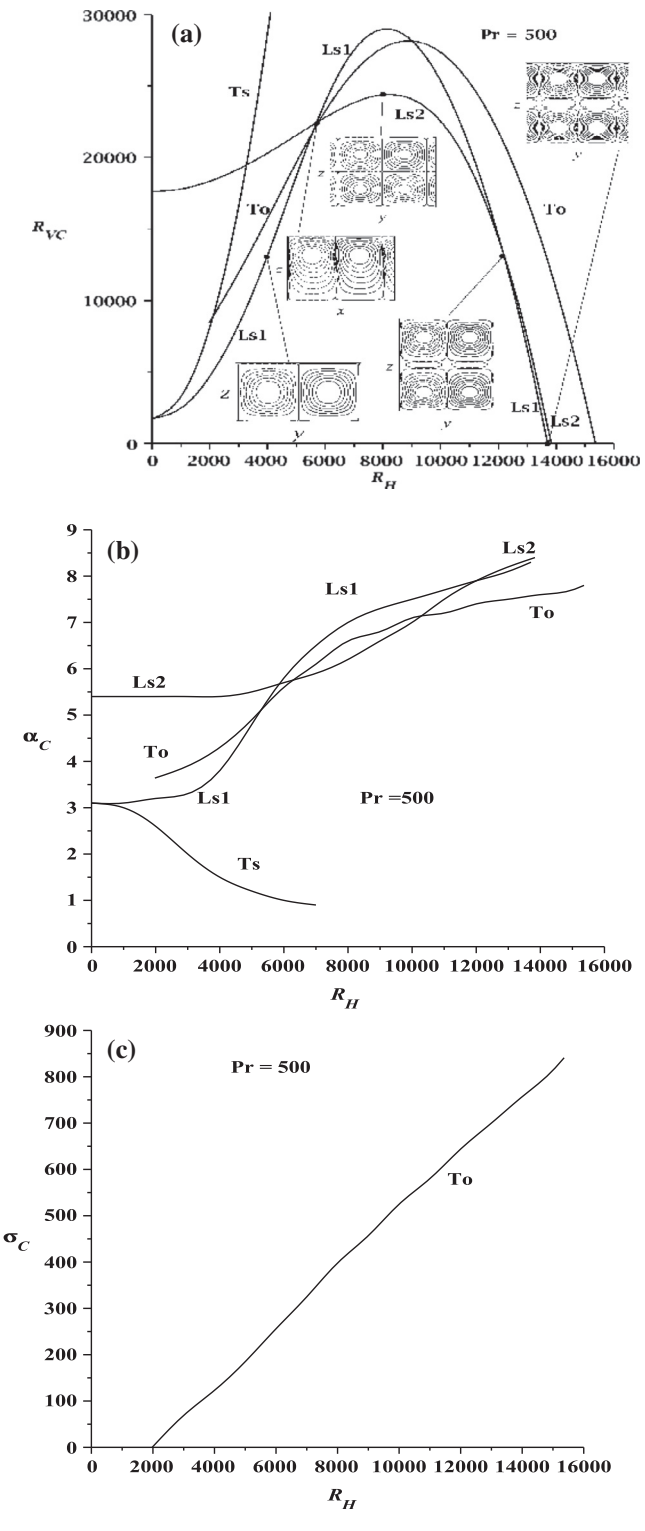

Fig. 5. Graphs of R_{VC}, α_C, and σ_C vs R_H for Pr = 500. In Fig. (a), *Ls*1 is the first unstable mode, then from R_H = 5564, the oscillatory transverse mode *To*, next from R_H= 5793, the mode *Ls*2 and from R_H= 12120, the mode *Ls*1. The first codimension two point occurs at R_H = 5564 and the second one at R_H = 5793. The *Ls*1 drops to R_{VC} = 0 at R_H = 13709.79. The critical wavenumbers and frequencies are shown in Figs. (b) and (c), respectively. The streamlines are ploted with the following data: *Ls*1 (4000, 13130.30, 3.8,0), *To* (5700, 22230.38, 5.4, 235.31), *Ls*2 (8000, 24390.58, 6.2, 0), *Ls*1 (12150, 13303.25, 8, 0) and *Ls*1 (13709.79, 0, 8.3, 0).

*Ls*1 (5564, 21754.60, 5.38,0) and *To* (5564, 21754.60, 5.29, 224.99) and the second one at *To* (5793, 22548.20, 5.44, 241.09) and *Ls*2 (5793, 22548.20, 5.62, 0). The intersection of *Ls*1 and *Ls*2 occurs now at *Ls*1 (12120, 13648.73, 7.94, 0) and *Ls*2 (12120, 13648.73, 7.91, 0). Notice that the last set of values are very close

to those of $Pr = 100$. In the range from $R_H = 0$ to $R_H = 5564$ the mode $Ls1$ is the first unstable one. To is the first unstable one in the range between the two codimension two points. $Ls1$ drops to $R_{VC} = 0$ at $R_{HC} = 13709.8$ with $\alpha_C = 8.3$. This figure also shows inserts with the streamlines of cell patterns of different modes of instability. The Fig. 5(b) and (c) present the critical wavenumbers and frequencies of oscillation, respectively. It is important to note that a decrease in the magnitude of the first unstable curves of criticality is observed in different regions of R_H when passing from $Pr = 2$ to $Pr = 500$. In that sense, the Prandtl number has a destabilizing effect on the flow. The results for Pr = 1000 are very similar to those of $Pr = 500$ and therefore they are omitted here. The mode To survives in a slightly shorter range of R_H as the first unstable one.

In natural convection the patterns appear due to vertical temperature gradients that are critical or larger than the critical one. However, in the present problem, the patterns are also determined by horizontal temperature gradients critical or larger than the critical one. This can be shown by the main temperature profile Eq. (11) which is modified by the main flow Eq. (9) (generated by the horizontal temperature gradient). This temperature profile (Eq. (11)) produces two unstable regions near the upper and lower walls and a stable region in the middle section (see Fig. 1 of Lappa [23] or here in Fig. 6). These unstable regions should be made more unstable by an adverse vertical temperature gradient. However, this is not possible because, in a range of R_H, the local vertical temperature gradients in the unstable regions are not large enough to destabilize the flow. Therefore, only after reaching a maximum of R_{VC}, the curves of criticality start to destabilize with R_H until $R_{VC} = 0$. The increase of R_H has an important influence on convection because the patterns change from a one-cell to a two-cell structure (mode $Ls2$) near the maximum of R_{VC}. In this case, the two unstable regions made by the temperature profile separate in such a way that two cells are able to form (see Fig. 6). Note that for this magnitude of R_H the two cells are in contact to each other. A further increase of R_H leads to a larger separation between the two unstable regions and consequently a three-cell structure appears. The reason is that for this magnitude of R_H, the two cells formed inside each unstable region of the temperature profile are so far away from each other that they can not touch directly, but only by means of a third cell in the middle generated by viscous friction. This pattern corresponds to the second even mode of instability.

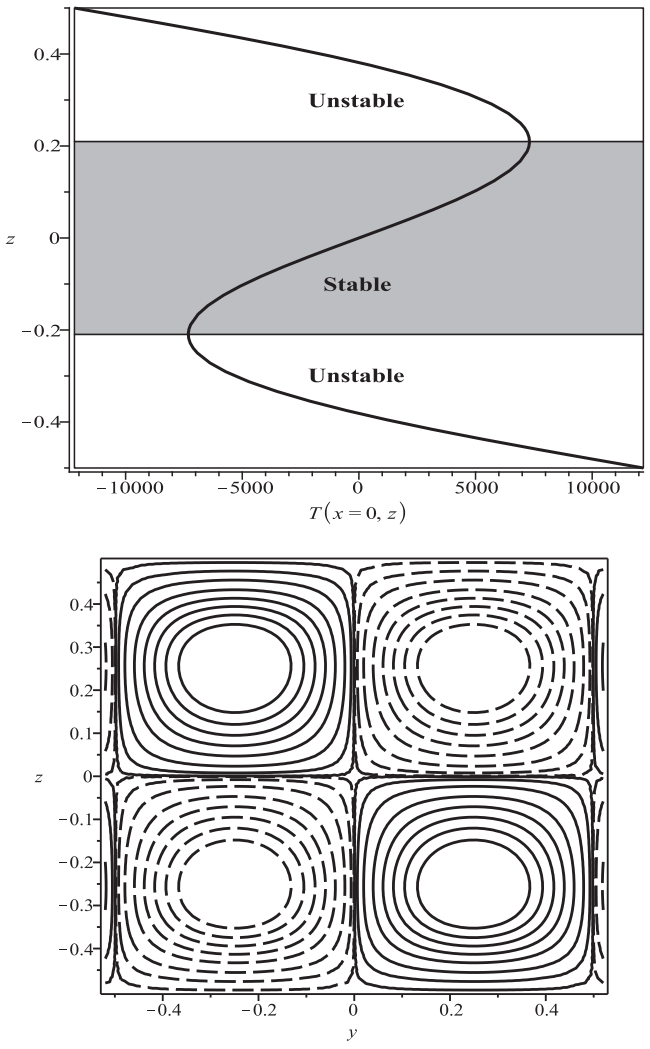

Fig. 6. Stable and unstable regions due to the main temperature profile for $Pr = 10$, $R_{VC} = 24388.3577$, $\alpha_C = 6.2$, $\sigma_C = 0$, and $R_H = 8000$. The corresponding streamlines of the convection cell are shown too. Note that under these conditions the two-cell pattern prevails (mode $Ls2$).

In [17] it was shown that to have a maximum and a minimum in the main temperature profile the inequality $R_H^2 \geqslant 5760R_V/7$ has to be satisfied. However, according to the numerical results, when R_H is large enough and satisfies the equality, the system is already located in the oscillatory mode $Lo1$ in the range $0.1 < Pr < 3$ (notice the strict inequalities). This might be a way to know when the oscillatory mode $Lo1$ appears as the first unstable one in that range of Pr. It is found that at the magnitudes of R_V and R_H of the first codimension two point, the slope of the temperature at $z = 0$ is negative and the profile still has no maximum and minimum. It is important to point out that the mode Obo appears in the range $0.45 \leqslant Pr \leqslant 2$ when $5225 \leqslant R_H \leqslant 8300$ (note that $R_H = 8300$ corresponds to $Pr = 0.45$ and $R_H = 5225$ to $Pr = 2$). However, it is possible that the Obo mode arises for the first time for $Pr > 0.2$. The occurance of the mode To as the first unstable one is more difficult to guess. But it is interesting to note that it always starts to appear in the picture above $Ls1$ for $R_H \simeq 2000$ in the range $Pr \geqslant 1$. The corresponding R_V decreases with Pr, as can be seen from Fig. 6 of [17] and following through all the figures in this paper. From the numerical analysis, it is possible to say that the codimension-two points between $Ls1$ and To can be found in the ranges $4538.5 \leqslant R_H \leqslant 5564$ and $17641.42 \leqslant R_V \leqslant 21754$ for $10 \leqslant Pr \leqslant 500$. The magnitudes at the right hand side of the inequalities are almost the same for $Pr = 1000$. The physical reason for the oscillatory motion is the propagation of internal waves in the stable region of the layer due to the shear flow.

All the physical points discussed above also depend on the magnitude of the Prandtl number. For example, in Ortiz-Pérez and Dávalos-Orozco [17] it is shown that for small Pr, R_H destabilizes immediately. When Pr increases, it is found that R_H first stabilizes and then destabilizes.

In this paper it is shown that, when Pr $\geqslant 10$, the qualitative and quantitative properties of the first unstable curves of criticality are similar and in some cases are almost the same. This improves whenever the Prandtl number is very large. Therefore, the idea is to use this result to obtain an approximate analytical formula which may be very useful and simple to write down for immediate applications. To attain this goal, the determinant obtained by the Galerkin method is expanded in terms of the small parameter 1/Pr. The expansion of the variables used is different from that presented above and is given in Appendix A. At zeroth order of 1/Pr, a very simple formula was found for each of the two most important modes $Ls1$ and $Ls2$ which fill almost all the range of R_H, when Pr is very large. The marginal curves of $Ls1$ are described by

Table 1
Mode Ls1.

Approximation order $1/Pr = 0$			High Galerkin, Pr = 10		High Galerkin, Pr = 100		High Galerkin, Pr = 500	
R_H	R_V	α	R_V	α	R_V	α	R_V	α
00000	01708.549	3.116	01708.831	3.1	01707.831	3.1	01707.831	3.1
01000	02448.781	3.121	02591.639	3.2	02464.627	3.1	02453.052	3.1
02000	04655.374	3.153	05188.937	3.5	04713.080	3.2	04668.501	3.2
03000	08281.082	3.267	09311.879	4.1	08379.135	3.4	08284.952	3.3
04000	13214.357	3.610	14569.875	4.8	13269.415	3.9	13130.307	3.8
05000	19122.244	4.486	20262.576	5.6	18844.137	4.9	18696.269	4.8
06000	25054.593	5.670	25347.823	6.3	24022.109	5.8	23889.425	5.8
07000	29577.447	6.561	28760.819	6.8	27645.490	6.5	27535.899	6.5
08000	31549.426	7.101	29918.547	7.2	29065.819	7.0	28983.998	7.0
09000	30625.723	7.399	28825.578	7.4	28241.067	7.3	28184.630	7.3
10000	27128.172	7.561	25731.060	7.6	25405.016	7.5	25371.923	7.5
11000	21569.087	7.653	20858.357	7.8	20782.529	7.7	20772.507	7.7
12000	14370.394	7.709	14321.664	8.0	14497.098	7.9	14510.168	7.9
13000	05817.140	7.744	06138.829	8.2	06577.316	8.1	06614.218	8.1
13611.54	00000.013	7.76	–	–	–	–	–	–
13641.77	–	–	00000.0007	8.3	–	–	–	–
13704.27	–	–	–	–	00000.004	8.3	–	–
13709.79	–	–	–	–	–	–	00000.005	8.3

Table 2
Mode Ls2

Approximation order $1/Pr = 0$			High Galerkin, Pr = 10		High Galerkin, Pr = 100		High Galerkin, Pr = 500.	
R_H	R_V	α	R_V	α	R_V	α	R_V	α
00000	17625.548	5.363	17611.755	5.4	17611.755	5.4	17611.755	5.4
01000	17810.270	5.365	17812.245	5.4	17798.017	5.4	17796.752	5.4
02000	18352.753	5.373	18399.477	5.4	18343.354	5.4	18338.364	5.4
03000	19217.378	5.393	19330.531	5.4	19207.241	5.4	19196.276	5.4
04000	20342.469	5.435	20530.716	5.5	20321.621	5.4	20302.791	5.4
05000	21635.340	5.512	21885.234	5.6	21578.326	5.5	21550.867	5.5
06000	22961.956	5.647	23232.582	5.7	22834.592	5.7	22799.115	5.7
07000	24127.435	5.868	24348.537	6.0	23880.844	5.9	23838.888	5.9
08000	24846.156	6.203	24920.669	6.3	24434.819	6.2	24390.587	6.2
09000	24719.491	6.650	24567.106	6.7	24130.697	6.6	24090.446	6.6
10000	23275.339	7.154	22885.767	7.2	22570.488	7.1	22540.614	7.0
11000	20088.103	7.636	19532.361	7.6	19398.582	7.5	19385.454	7.5
12000	14879.801	8.049	14278.519	8.0	14375.128	7.9	14382.591	7.9
13000	07531.651	8.383	06995.599	8.2	07355.395	8.2	07386.127	8.2
13766.51	–	–	−0000.002	8.5	–	–	–	–
13810.81	00000.001	8.600	–	–	–	–	–	–
13827.02	–	–	–	–	0000.002	8.4	–	–
13832.39	–	–	–	–	–	–	00000.004	8.4

$$R_V = \frac{59}{205920}R_H^2 + 20880 + \frac{14}{13}\alpha^4 + \frac{2388}{13}\alpha^2 + \frac{939168}{\alpha^2} - \frac{1}{31409664}\left[465910016R_H^4 - 729\{24146744573952 + \frac{25797804032}{243}\alpha^4 + \frac{12898902016000}{81}\alpha^2 + \frac{10425261149388800}{9\alpha^2}\right\}R_H^2 + 674235560957072338059264 + 5837674512384\alpha^8 + 22416670127554560\alpha^6 + 2578197273045368832\alpha^4 + 6092911465678673805312\alpha^2 + \frac{3708608938368526140309504}{\alpha^2} + \frac{8608312990277068124313354 24}{\alpha^4}\right]^{1/2} \quad (18)$$

and those of *Ls*2 are described by

$$Rv = \frac{1}{(C_5\alpha)^2}\left\{-C_5C_0\alpha^2R_H^2 + C_1\alpha^6 + C_2\alpha^4 + C_3\alpha^2 + C_4 - \left[\alpha^4C_5^2C_6R_H^4 - \alpha^2(C_7\alpha^6 + C_8\alpha^4 + C_9\alpha^2 + C_{10})C_5R_H^2 + C_{11}\alpha^{12} + C_{12}\alpha^{10} + \alpha^8C_{13} + \alpha^6C_{14} + \alpha^4C_{15} + \alpha^2C_{16} + C_{17}\right]^{1/2}\right\} \quad (19)$$

The seventeen coefficients C_i are given in Appendix A.

For fixed R_H, the critical R_{VC} is calculated varying α and selecting the lowest value (the minimum) obtained from each of the formulas Eqs. (18) and (19). The two calculated critical curves also cross to each other at a point very near to that shown in the figures from Fig. 3(a) to Fig. 5(a) using a high order Galerkin approximation. The crossing point of this approximate curves occurs at $R_H = 11710$ and $R_V = 16607$ with $\alpha = 7.695$ for *Ls*1 and $\alpha = 7.937$ for *Ls*2. These show the maximum errors of 3.5% and 21.6%, respectively, for $Pr = 500$. The wavenumber errors are minimal for all Prandtl numbers and are around 3.2% and 0.3%, respectively. If, as shown in Appendix A, the curves are a very good approximation why is there a maximum error of 21.6 % for R_V at the crossing point? The reason is that around the crossing point both curves are very near to each other in a range of R_H and a slight displacement (slight error) means a large change in R_V for this point. Note that the formulae are a better approximation for large Prandtl numbers.

Notice that the results presented above are in contrast with those of Fig. 6.8 of Lappa [24] for horizontal temperature gradient alone, that is, for $R_V = 0$. In that figure a dashed curve appears for the *Ls*2 mode which appears as the first unstable one (before the mode *Ls*1). This is pointed out here in order to avoid any confusion (see Appendix B for the validation and convergence of the numerical algorithm). In the present paper it has been shown by means of a high precision numerical analysis, that the oblique mode appears

Table 3
Convergence of the Galerkin Method: Pr = 10 and Pr = 500

Order	Ls1				Ls2			
	R_H	R_V	α	Error (%)	R_H	R_V	α	Error (%)
Pr = 10								
2	14138.030	−0.0035	7.6	2.404	13740.292	−0.0023	8.6	0.377
3	13806.127	−0.0010	8.4	1.204	13792.155	0.0012	8.4	0.186
4	13641.770	−0.0034	8.3	0.124	13766.510	−0.0019	8.5	0.080
5	13624.821	0.0033	8.3	0.024	13755.430	−0.0020	8.5	0.014
6	13621.419	−0.0012	8.3	0.007	13753.481	0.0025	8.5	0.004
7	13620.461	−0.0058	8.3	–	13752.914	0.0014	8.5	–
Pr = 500								
2	14179.835	−0.0015	7.6	2.202	13809.392	0.0021	8.6	0.351
3	13874.293	−0.0010	8.3	1.199	13857.954	0.0053	8.4	0.184
4	13709.799	−0.0043	8.3	0.126	13832.385	0.0036	8.4	0.080
5	13692.521	0.0032	8.3	0.025	13821.323	0.0031	8.4	0.014
6	13689.093	0.0016	8.3	0.007	13819.379	−0.0011	8.4	0.004
7	13688.128	0.0014	8.3	–	13818.815	0.0010	8.4	

and disappears with Pr and that the transverse oscillatory mode reduces considerably its range in R_H but never disappears increasing Pr. Furthermore, it is also shown that the stationary *Ls*1 mode remains the first unstable one after crossing the curve of *Ls*2 when R_H increases. Therefore, *Ls*1 is the first unstable mode when $R_{VC} = 0$, as has been the case for all the Prandtl numbers investigated $0.26 \leqslant Pr \leqslant 1000$. However, *Ls*2 starts to become important somewhere inside the range $0.5 < Pr < 1$ (see reference [17]).

Nonlinear problems on convection under an inclined temperature gradient are hardly found under the conditions of the present paper. One exception is the paper by Kaloni and Qiao [16]. They used the nonlinear energy method to determine sufficient conditions for stability. They show, for the first time, that the curves of criticality have to drop down with R_H until $R_V = 0$ when Pr is large. However, there are some papers on nonlinear convection under a horizontal temperature gradient. Wang and Korpela [7] calculated the nonlinear supercritical instability for finite aspect ratio. Laure and Roux [9] investigated the linear and weakly nonlinear stability. Gelfgat et al. [25] investigated linear and supercritical instabilities for the case for aspect ratios from 1 to 11 and various Pr. Few experiments are found like that of Hung and Andereck [26] who made experiments for convection near and far above the criticality. Wang and Huang [27] made experiments with small aspect ratio where the temperature gradients produce magnitudes of R_H above the critical R_{HC}. All this means that the nonlinear stability calculations of a system under the same conditions as in the present paper are still an open problem.

5. Conclusions

In this paper the range $2 \leqslant Pr \leqslant 500$ is covered to investigate the instability of convective flows under an inclined temperature gradient (however, larger magnitudes of *Pr* were also investigated but the results were similar). It is shown that the oblique oscillatory mode *Obo* found by Ortiz-Pérez and Dávalos-Orozco [17] disappears somewhere in the range $2 \leqslant Pr \leqslant 10$. However, it is believed that it is also replaced as the first unstable one by the transverse oscillatory mode *To* with a small increase of Pr above 2. It is also shown that the transverse oscillatory mode found by Nield [15] decreases its range considerably with *Pr*, but never disappears. It is found that, for $Pr \geqslant 0.5$ the longitudinal modes *Ls*1 and *Ls*2 play important roles on the instability for almost all the range of R_H investigated, except in the short range where the Obo and To modes are present. Simple and useful formulas, Eqs. (18) and (19), were obtained to calculate the curves of criticality for both *Ls*1 and *Ls*2. They are good approximations for Pr = 10 and very good approximations for $Pr \geqslant 100$. The results of these two formulas also agree with the high order Galerkin method in the result that *Ls*1 becomes the first unstable mode after crossing the curve of *Ls*2 with an increase of R_H. Further, the main temperature profile is used to understand the changes in cell structure when R_H is increased. The growth of R_H increases the stable region in the middle of the liquid layer and consequently increases the separation between the unstable regions formed near each of the two walls. At the same time, R_H increases the local temperature gradient at the two unstable regions. The larger separation between the unstable regions due to the increase of R_H is responsible for the creation of the observed two-cell structure (*Ls*2) and three-cell structure (*Ls*1) found in the present convection problem.

Acknowledgments

The authors would like to thank Joaquín Morales, Caín González, Alberto López, Alberto López, Raúl Reyes, Ma. Teresa Vázquez and Oralia Jiménez for technical support. A. S. Ortiz-Pérez would like to thank the support from Instituto para la Planeación del Desarrollo, A. C (IPD).

Appendix A

In this Appendix the calculations leading to formulas Eqs. (18) and (19) are presented. Those formulas correspond to the first and second longitudinal stationary modes *Ls*1 and *Ls*2 which dominate almost all the range of R_H for large Pr. Therefore, they were obtained assuming $\sigma = 0$, $k = 0$ and $Pr \to \infty$. Under these assumptions, Eqs. (12)–(14) can be reduced to:

$$(D^2 - \alpha^2)^2 w - \alpha^2 \theta = 0 \tag{A.1}$$

$$(D^2 - \alpha^2)\theta - wDT = 0 \tag{A.2}$$

Notice that under the present conditions Eq. (14) decouples from the other two. This system of equations can be written as:

$$\begin{bmatrix} L_1^2 & -\alpha^2 \\ -DT & L_1 \end{bmatrix} \begin{bmatrix} w \\ \theta \end{bmatrix} = \begin{bmatrix} 0 \\ 0 \end{bmatrix} \tag{A.3}$$

where the operator is defined as $L_1 = (D^2 - \alpha^2)$.

The general problem is solved using the expansions

$$w = \sum_{n=1}^{N} A_n W_n = w_e + w_o = \sum_{n=1}^{N} [a_{2(n-1)} z^{2(n-1)} (z^2 - 1/4)^2 + b_{2n-1} z^{2n-1} (z^2 - 1/4)^2] \tag{A.4}$$

$$\theta = \sum_{n=1}^{N} B_n T_n = \theta_e + \theta_o = \sum_{n=1}^{N} [c_{2n-1} z^{2(n-1)} (z^2 - 1/4)^2 + d_{2n} z^{2n-1} (z^2 - 1/4)^2] \tag{A.5}$$

$$u = \sum_{n=1}^{N} C_n U_n = u_e + u_o = \sum_{n=1}^{N} [f_{2n-1} cos(2n-1)\pi z + g_{2n} sin 2n\pi z] \tag{A.6}$$

Notice that the selection of the expansion functions for θ is because this gave the best approximate formulas Eqs. (18) and (19). These expansions include even and odd functions where A_n, B_n and C_n are the coefficients of the basic functions W_n, T_n and U_n.

The solution of the complete system of Eqs. (12)–(14), by the second order Galerkin method needs the solution of the following determinant

$$det(M)=\begin{vmatrix} \langle L_1W_1,W_1\rangle & -\alpha^2\langle T_1,W_1\rangle & 0 & \langle L_1W_2,W_1\rangle & -\alpha^2\langle T_2,W_1\rangle & 0\\ \langle DTW_1,T_1\rangle & \langle L_2T_1,T_1\rangle & -R_H\langle U_1,T_1\rangle & \langle DTW_1,T_1\rangle & \langle L_2T_1,T_1\rangle & -R_H\langle U_1,T_1\rangle\\ \langle L_4W_1,U_1\rangle & \mathbf{0} & \langle L_3U_1,U_1\rangle & \langle L_4W_2,U_1\rangle & 0 & \langle L_3U_2,U_1\rangle\\ \langle L_1W_1,W_2\rangle & -\alpha^2\langle T_1,W_2\rangle & 0 & \langle L_1W_2,W_2\rangle & -\alpha^2\langle T_2,W_2\rangle & 0\\ \langle DTW_1,T_2\rangle & \langle L_2T_1,T_2\rangle & -R_H\langle U_1,T_2\rangle & \langle DTW_1,T_2\rangle & \langle L_2T_1,T_2\rangle & -R_H\langle U_1,T_2\rangle\\ \langle L_4W_1,U_2\rangle & \mathbf{0} & \langle L_3U_1,U_2\rangle & \langle L_4W_2,U_2\rangle & 0 & \langle L_3U_2,U_2\rangle \end{vmatrix}$$

where: $\langle f,g\rangle=\int_{-1/2}^{1/2}fgdz$. If only longitudinal modes are needed, then the even (odd) mode only requires the even (odd) functions of Eqs. (A.4) and (A.5). This means a great simplification of the determinant. However, when the limit $Pr\to\infty$ is taken, the determinant reduces to:

$$det(M)=\begin{vmatrix} \langle L_1W_1,W_1\rangle & -\alpha^2\langle T_1,W_1\rangle & \langle L_1W_2,W_1\rangle & -\alpha^2\langle T_2,W_1\rangle\\ \langle DTW_1,T_1\rangle & \langle L_2T_1,T_1\rangle & \langle DTW_1,T_1\rangle & \langle L_2T_1,T_1\rangle\\ \langle L_1W_1,W_2\rangle & -\alpha^2\langle T_1,W_2\rangle & \langle L_1W_2,W_2\rangle & -\alpha^2\langle T_2,W_2\rangle\\ \langle DTW_1,T_2\rangle & \langle L_2T_1,T_2\rangle & \langle DTW_1,T_2\rangle & \langle L_2T_1,T_2\rangle \end{vmatrix}$$

In the case of $Ls1$ only the w_e and θ_e are used for w and θ, that is

$$w_e=\sum_{n=1}^{N}\left[a_{2(n-1)}z^{2(n-1)}(z^2-1/4)^2\right] \tag{A.7}$$

$$\theta_e=\sum_{n=1}^{N}\left[c_{2(n-1)}z^{2(n-1)}(z^2-1/4)^2\right] \tag{A.8}$$

and from them Eq. (18) is obtained. For $Ls2$ the terms w_o and θ_o are used, that is

$$w_o=\sum_{n=1}^{N}\left[b_{2n-1}z^{2n-1}(z^2-1/4)^2\right] \tag{A.9}$$

$$\theta_o=\sum_{n=1}^{N}[d_{2n}sin2n\pi z] \tag{A.10}$$

which lead to Eq. (19).

In the following Tables 1 and 2, one for $Ls1$ and the other for $Ls2$, are presented the numerical comparisons between the approximate formulas and the high order Galekin method. There, it is shown the effectiveness of the simple Eqs. (18) and (19) for different Prandtl numbers. In each table three lines are added to show the different magnitudes of R_H where R_V becomes zero for the different values of Pr.

Due to their large extension, the seventeen coefficients of Eq. (19) for the marginal values of R_V of the odd mode $Ls2$ are presented here. They are:

$$C_0=45\sqrt{2}\left(128\pi^8+23520\pi^6-1522080\pi^4+17222625\pi^2-45544275\right)/\left(2097152\pi^2\right)$$

$$C_1=225\pi^{14}\left(6656\pi^8+4227084225-1184256\pi^6+64944000\pi^4-960172920\pi^2\right)/67175972864$$

$$C_2=45\pi^{14}\left(-22165272675\pi^2+464979264750+1155818880\pi^6-22717440\pi^8-11843559000\pi^4+131584\pi^{10}\right)/16793993216$$

$$C_3=405\pi^{14}\left(154926872100\pi^2-123788800\pi^8+789504\pi^{10}+6234869760\pi^6-77816466000\pi^4+1162448161875\right)/8396996608$$

$$C_4=2025\pi^{16}\left(131584\pi^8-15896727000\pi^2+1046209920\pi^4-18368000\pi^6+71531997075\right)/161480704$$

$$C_5=2025\sqrt{2}\pi^2\left(8\pi^4-105\pi^2+315\right)/8192$$

$$C_6=28704375\left(36608\pi^{12}-102290060250\pi^2-3501792000\pi^6+201081888\pi^8+28111511295\pi^4-4707840\pi^{10}+136903411575\right)/\left(21990232555552\pi^4\right)$$

$$C_7=91125\sqrt{2}\pi^{12}\left(10215424\pi^{14}-493240320\pi^{12}-7266823178288625\pi^2-145483738772400\pi^6+6386414025600\pi^8+1495248208587000\pi^4-86045137920\pi^{10}+13759367056036875\right)/70439112921841664$$

$$C_8=91125\pi^{12}\sqrt{2}\left(-1618845696\pi^{14}-360751242240\pi^{12}-104977386498859875\pi^2+2775821144607000\pi^6-441635595332400\pi^8+3872553785706375\pi^4+40099840\pi^{16}+23733268272000\pi^{10}+302706075232811250\right)/17609778230460416$$

$$C_9=820125\pi^{12}\sqrt{2}\left(-10949238784\pi^{14}-1709120000000\pi^{12}-129809431450573875\pi^2+21380010774343200\pi^6-2511913849704000\pi^8-603791557448625000\pi^4+240599040\pi^{16}+121130655663360\pi^{10}+756765188082028125\right)/8804889115230208$$

$$C_{10}=4100625\pi^{14}\sqrt{2}\left(40099840\pi^{14}-1976418304\pi^{12}-24551372029944375\pi^2-487456817778000\pi^6+21062606947200\pi^8+5040655848509400\pi^4-267202790400\pi^{10}+46573139073124125\right)/169324790677504$$

$$C_{11}=50625\pi^{28}\left(6656\pi^8-1202688\pi^6+65185920\pi^4-960898680\pi^2+4227084225\right)\times\left(6656\pi^8-1165824\pi^6+64702080\pi^4-959447160\pi^2+4227084225\right)/4512611330224864362496$$

$$C_{12} = 10125\pi^{28}(43137739653120\pi^{14} - 3049297844428800\pi^{12} - 5401549728417766218 75\pi^{2} + 875823104\pi^{18} + 1426753714541853600 0\pi^{6} - 1945656141136243200\pi^{8} + 1416249590948010000\pi^{4} + 1965506514976823568750 - 307036422144\pi^{16} + 111311915165107200\pi^{10})/ 564076416278108045312$$

$$C_{13} = 2025\pi^{28}(4373251995823432440468 75 + 17314349056\pi^{20} - 44863191486259200\pi^{14} + 1116802837908403200\pi^{12} - 4136958828122372752500 0\pi^{2} - 5742031011840\pi^{18} + 6539021006679800730000\pi^{6} - 4603677884887944240 00\pi^{8} - 2862175509453915683437 5\pi^{4} + 741071559720960\pi^{16} + 1664944356200832000\pi^{10})/28203820813905402265 6$$

$$C_{14} = 18225\pi^{28}(51943047168\pi^{20} - 146105627844403200\pi^{14} + 4788897028163136000\pi^{12} + 7227131496828446640937 5\pi^{2} - 16969746350080\pi^{18} + 6020211271324882905000\pi^{6} + 8187931639824300000 0\pi^{8} - 4877282955285650534625 0\pi^{4} + 2227163326382080\pi^{16} - 6488796973486464000 0\pi^{10} + 2702571458093132407031 25)/352547760173817528 32$$

$$C_{15} = 18225\pi^{28}(10111579848704\pi^{20} - 276464152795299840 00\pi^{14} + 9920213915442518016 00\pi^{12} + 1188953304412687713900000 0\pi^{2} - 3164780049203200\pi^{18} - 8872323555000545640000 0\pi^{6} + 1314940944772116305280 00\pi^{8} - 3746285613890572725472500\pi^{4} + 1216157156141909583164062 5 + 410267312522526720\pi^{16} - 1736165943746777088000 0\pi^{10})/705095520347635056 64$$

$$C_{16} = 820125\pi^{30}(3918986036510720\pi^{14} - 266802378135552000\pi^{12} - 7396892519082584017500\pi^{2} + 103886094336\pi^{18} + 1823764386552326064000\pi^{6} - 1920757407538233600 00\pi^{8} - 6813050918038214850000\pi^{4} - 307902349312 00\pi^{16} + 9997031016085478400\pi^{10} + 8315223851508162651562 5)/ 677976461872726016$$

$$C_{17} = 4100625\pi^{32}(-4833869824000\pi^{14} + 612421730959360\pi^{12} - 2274249258532147050000\pi^{2} - 3589012598060736000 0\pi^{6} + 1697289330860928000\pi^{8} + 4023804485423756880 00\pi^{4} + 17314349056\pi^{16} - 4260944750899200 0\pi^{10} + 5116826605537808555625)/2607601776433561 6$$

Appendix B

In this appendix a discussion is presented on the validation of the numerical algorithm used in the paper. This will be done in two ways. One is to show the convergence of the algorithm by means of two examples corresponding to Pr = 10 and 500. Besides, a comparison is done with Figs. 3 and 5 of Birikh and Katanova [28] and of Fig. 10 of Gershuni et al. [29] where R_V = 0. Notice that this Fig. 10 of [29] is the same as Fig. 6.8 of Lappa [24]. The curve 1 of Fig. 3 of [28] corresponds to the oscillatory mode *To* of Ortiz -Pérez and Dávalos-Orozco [17]. It is important to point out that both papers have no numerical tables. Therefore, their figures are amplified and copied to calculate the magnitudes of the critical parameters with the best precision possible. The critical value that [29,28] find is R_{HGBK} = 1269 with a wavenumber α_{GBK} = 4.15, which have to be multiplied by 16 and 2, respectively, in order to be able to compare due to the different scaling. The results are $R_{HGBK} \cdot 16$ = 20304, $\alpha_{BK} \cdot 2$ = 8.3 and those of [17] are R_H = 20281.2, α = 8.2. As can be seen, the agreement is very good. The extra subindexes *GBK* mean data of the papers [29,28]. Notice that α_{BK} only has the extra subindex *BK* because Gershuni et al. [29] did not give graphs for the wavenumber for Pr = 1. Moreover, in both papers there are no numerical results of the frequency of oscillation.

The first draft of paper [17] contained results for Pr = 0.1 but, due to the length of the paper, they were deleted. For this reason, we are able to compare that data with the results of [29,28] for the T_S mode. They find R_{HBK} = 79 and α_{BK} = 1.3 and multiplication gives $R_{HGBK} \cdot 16$ = 1230 and $\alpha_{BK} \cdot 2$ = 2.6. The agreement is good with the values R_H = 1278 and α = 2.6 of [17].

However, disagreement is found with the results of Gershuni et al. [29] for magnitudes of $Pr \geqslant 10$. In [17] it is found that the mode *Ls*2 is never the first unstable one when R_V = 0. This is clearly shown in Figs. 1–6for Pr = 0.026 to Pr = 1, respectively. In the present paper it is shown that the same condition prevails from Pr = 2 to Pr = 1000 (not shown but calculated too). Note that with respect to mode *Ls*2, comparison is very difficult with [28] due to the scaling of their Fig. 5. However, they make a very important comment in their Section 4. They say that "The results are in good agreement with those in [29], except for the curve of the spiral monotonic mode (the upper curve 5 corresponding to the odd mode (*Ls*2) does not intersect the lower curve of the even mode (*Ls*1))". The parenthesis with *Ls*1 and *Ls*2 were added here. They attribute the differences to the "insufficient accuracy of the calculations on this range of the parameters". Even more, Gershuni et al. [29] limit their calculations to a range of $Pr \leqslant 100$, as can be seen in their Fig. 10. In this sense, our results are in agreement with those of Birikh and Katanova [28]. Therefore, in what follows, it will be shown that the numerical algorithm used in this paper has a very good convergence and that the agreement with [28] is not fortuitous.

The convergence of the numerical Galerkin method used here and in [17] will be understood by means of the calculated error between orders of approximation. This is given in Table 3. Two examples of Pr = 10 and 500 are presented for the particular cases of *Ls*1 and *Ls*2 when R_V = 0. The critical value of R_H is localized where R_V is very near to zero. Therefore, the column of R_V sometimes shows very small positive and negative values. The error is calculated with respect to the next value. As can be seen, the convergence is very good and the difference between the results of the fourth, fifth and sixth order is very small (less than one percent).

In this way, it is concluded that the results agree very well with [28] in the limit of R_V = 0. The percentage of the errors shown in Table 3 support the reliability of the numerical results presented in this paper and in [17] for all Prandtl numbers. The numerical algorithm is able to distinguish clearly between modes *Ls*1 and *Ls*2.

References

[1] D.T.J. Hurle, E. Jakeman, C.P. Johnson, Convective temperature oscillations in molten gallium, J. Fluid Mech. 64 (1974) 565–576.
[2] A.E. Gill, A theory of thermal oscillations in liquid metals, J. Fluid Mech. 64 (1974) 577–588.
[3] S. Chandrasekhar, Hydrodynamic and Hydromagnetic Stability, Dover Publications Inc.,, New York, 1981.
[4] J.E. Hart, Stability of thin non-rotating hadley circulations, J. Atmos. Sci. 29 (1972) 687–697.
[5] H.P. Kuo, S.A. Korpela, A. Chait, P. Marcus, Stability of natural convection in a shallow cavity, Proc. Eighth Int. Heat Transfer Conf. 4 (1986) 1539–1544.
[6] H.P. Kuo, S.A. Korpela, Stability and finite amplitude natural convection in a shallow cavity with insulated top and bottom and heated from a side, Phys. Fluids 31 (1988) 33–42.

[7] T.-M. Wang, S.A. Korpela, Convection rolls in a shallow cavity heated from the side, Phys. Fluids A 1 (1989) 947–953.
[8] P. Laure, Study of convective motions in a rectangular cavity with horizontal gradient of temperature, J. Theor. Appl. Mech. 6 (1987) 351–382.
[9] P. Laure, B. Roux, Linear and non-linear analysis of the hadley circulation, J. Cryst. Growth 97 (1989) 226–234.
[10] G.O. Hughes, R.W. Griffiths, Horizontal convection, Annu. Rev. Fluid Mech. 40 (185) (2008).
[11] J.E. Weber, On thermal convection between non-uniformly heated planes, Int. Heat Mass Transfer 16 (1973) 961–970.
[12] D. Sweet, E. Jakeman, D.T.J. Hurle, Free convection in the presence of both vertical and horizontal temperature gradients, Phys. Fluids 20 (1977) 1412–1415.
[13] S.P. Bhattacharyya, S. Nador, Stability of thermal convection between non-uniformly heated plates, Appl. Sci. Res. 32 (1976) 555–570.
[14] J.E. Weber, On the stability of thermally driven shear flow heated from below, J. Fluid Mech. 87 (1978) 65–84.
[15] D.A. Nield, Convection induced by an inclined temperature gradient in a shallow horizontal layer, Int. J. Heat and Fluid Flow 15 (1994) 157–162.
[16] P.N. Kaloni, N. Qiao, On the nonlinear stability of thermally driven shear flow heated from below, Phys. Fluids 8 (1996) 639–641.
[17] A.S. Ortiz-Pérez, L.A. Dávalos-Orozco, Convection in a horizontal fluid layer under an inclined temperature gradient, Phys. Fluids 23 (2011) 084107.
[18] M. Lappa, Exact solutions for thermal problems: Buoyancy, Marangoni, vibrational and magnetic-field-controled flows, Rev. Appl. Phys. 1 (2012) 1–14.
[19] B.A. Finlayson, The Galerkin method applied to convective instability problems, J. Fluid Mech. 17 (1968) 201–208.
[20] B.A. Finlayson, The Method of Weighted Residuals and Variational Principles, Mathematics in Science and Engineering, Academic Press, New York, USA, 1972.
[21] J.E. Hart, A note of stability of low-Prandtl-number Hadley circulations, J. Fluid Mech. 132 (1983) 271–281.
[22] W.M. Kays, Convective Heat and Mass Transfer, Appendix A. Property Values, McGraw-Hill, New York, USA, 1980 (pp. 387–399).
[23] M. Lappa, Secondary and oscillatory gravitational instabilities in canonical three-dimensional models of crystal growth from the melt. ii: lateral heating and the Hadley circulation, C.R. Mec. 335 (2007) 261–268.
[24] M. Lappa, Thermal Convection, John Wiley & Sons, London, 2010.
[25] A. Yu. Gelfgat, P.Z. Bar-Yoseph, A.L. Yarin, Stability of multiple steady states of convection in laterally heated cavities, J. Fluid Mech. 388 (1999) 315–334.
[26] M.C. Hung, C.D. Andereck, Transitions in convection driven by a horizontal temperature gradient, Phys. Lett. A 132 (1988) 253–258.
[27] W. Wang, R.X. Huang, An experimental study on thermal circulation driven by horizontal differential heating, J. Fluid Mech. 540 (2005) 49–73.
[28] R.V. Birikh, T.N. Katanova, The effect of high frequency vibrations on the stability of advective flow, Fluid Dyn. 33 (1992) 12–17.
[29] G.Z. Gershuni, P. Laure, V.M. Myznikov, B. Roux, E.M. Zhukhovitsky, On the stability of plane-parallel advective flows in long horizontal layers, Microgravity Q. 2 (1998) 141–151.